Available online at www.sciencedirect.com
ScienceDirect
Remote Sensing of Environment 112 (2008) 2131–2144
Remote Sensing of Environment
www.elsevier.com/locate/rse

A systematic method for 3D mapping of mangrove forests based on Shuttle Radar Topography Mission elevation data, ICEsat/GLAS waveforms and field data: Application to Ciénaga Grande de Santa Marta, Colombia

Marc Simard [a,*], Victor H. Rivera-Monroy [b], José Ernesto Mancera-Pineda [c], Edward Castañeda-Moya [b], Robert R. Twilley [b]

[a] Radar Systems, MS 300-319D, Jet Propulsion Laboratory, Pasadena, CA 91109, USA
[b] Wetland Biogeochemistry Institute, Louisiana State University, Baton Rouge, LA, 70803, USA
[c] Universidad Nacional de Colombia - Sede Caribe, San Andres, Colombia

Received 2 November 2006; received in revised form 2 October 2007; accepted 28 October 2007

Abstract

Mangrove forests are found within the intertropical zone and are one of the most biodiverse and productive wetlands on Earth. We focus on the Ciénaga Grande de Santa Marta (CGSM) in Colombia, the largest coastal lagoon–delta ecosystem in the Caribbean area with an extension of 1280 km^2, where one of the largest mangrove rehabilitation projects in Latin America is currently underway. Extensive man-made hydrological modifications in the region caused hypersaline soil (>90 g kg^{-1}) conditions since the 1960s triggering a large dieback of mangrove wetlands (~247 km^2). In this paper, we describe a new systematic methodology to measure mangrove height and aboveground biomass by remote sensing. The method is based on SRTM (Shuttle Radar Topography Mission) elevation data, ICEsat/GLAS waveforms (Ice, Cloud, and Land Elevation Satellite/Geoscience Laser Altimeter System) and field data. Since the locations of the ICEsat and field datasets do not coincide, they are used independently to calibrate SRTM elevation and produce a map of mangrove canopy height. We compared height estimation methods based on waveform centroids and the canopy height profile (CHP). Linear relationships between ICEsat height estimates and SRTM elevation were derived. We found the centroid of the canopy waveform contribution (CWC) to be the best height estimator. The field data was used to estimate a SRTM canopy height bias (−1.3 m) and estimation error (rms = 1.9 m). The relationship was applied to the SRTM elevation data to produce a mangrove canopy height map. Finally, we used field data and published allometric equations to derive an empirical relationship between canopy height and biomass. This relationship was used to scale the mangrove height map and estimate aboveground biomass distribution for the entire CGSM. The mean mangrove canopy height in CGSM is 7.7 m and most of the biomass is concentrated in forests around 9 m in height. Our biomass maps will enable estimation of regeneration rates of mangrove forests under hydrological rehabilitation at large spatial scales over the next decades. They will also be used to assess how highly disturbed mangrove forests respond to increasing sea level rise under current global climate change scenarios.

Keywords: Radar; SRTM; Lidar; ICEsat; GLAS; Mangroves; Mangrove; Wetlands; Forest; Height; Waveforms

1. Introduction

Mangroves are found between latitudes 31° north and 38° south, particularly along the tropical and subtropical coasts of Australia, Asia, Africa and the Americas. The mangrove forest is one of the most productive ecosystems on Earth with a mean production of 2.5 g C m^{-2} per day (Jennerjahn & Ittekkot, 2002). The combination of shallow waters, high levels of nutrients, and high primary productivity makes these areas ideal for supporting intricate food webs in several types of environmental settings (Twilley & Rivera-Monroy, 2005). Mangrove wetlands generate ample goods and services to society such as providing critical habitat for bird, fish and other wildlife, playing key roles in biogeochemical hydrologic cycles, regulating water quality, reducing shoreline erosion, offering

* Corresponding author. Tel.: +1 818 354 6972; fax: +1 818 393 5184.
E-mail addresses: marc.simard@jpl.nasa.gov (M. Simard), vhrivera@lsu.edu (V.H. Rivera-Monroy), jemancerap@unal.edu.co (J.E. Mancera-Pineda).

0034-4257/$ - see front matter © 2008 Elsevier Inc. All rights reserved.
doi:10.1016/j.rse.2007.10.012

flood protection (as result of tropical storms, hurricanes, and tsunamis (Kathiresan & Rajendran, 2006)), moderating climate, and supporting numerous economic activities such as hunting, fishing, and recreation (Ewel et al., 1998).

Because mangroves couple biogeochemical processes between land and sea, landscape degradation in these coastal zones magnifies regional impacts. A recent United Nations Environment Programme report (UNEP, 2006) estimates that their economical value varies geographically between $200 k and $900 k per km^2 per year. The primary drivers of mangrove conversion are related to human impacts: urban expansion, shrimp farming, water management practices, charcoal cut as well as natural hazards such as sea level rise, hurricanes, severe storms and tsunamis. Among the major impacts of mangrove loss are decline in biodiversity, degradation of clean water supplies, siltation of coral reefs and acidification of coastal soils, erosion, loss of shoreline stability, release of more carbon into the atmosphere, and reduction (or disappearance) of important commercial fish stocks (Sanchez-Ramirez & Rueda, 1999; Rueda & Defeo, 2001). It is estimated that the loss of original mangrove forests is as high as 35% and may reach 60% by 2030 (Valiela et al., 2001; UNEP, 2006; Alongi, 2002). These are, however, gross estimates and do not rely on accurate landscape analyses, which can only be improved through remote sensing landscape scale assessment.

Both radar and optical remote sensing have been used extensively to map mangroves with varying degrees of success (e.g. Kovacs et al., 2005; Laba et al., 1997, Ramsey et al., 1996; Rasolofoharinoro et al., 1998; Wang et al., 2004; Held et al., 2003; Simard et al., 2000; Mougin et al., 1999). Recently, structural (tree height) and functional (biomass) attributes of mangroves have been estimated using radar interferometry (Simard et al., 2006). In February of 2000, Space Shuttle Endeavour collected nearly global coverage of Earth's topography using radar interferometry (SRTM, Shuttle Radar Topography Mission). And because of limited penetration of microwaves within vegetation, the SRTM topographic maps contain information related to vegetation height (Kellndorfer et al., 2004). Mangrove forests are located within the intertidal zone (i.e. at sea level), which particularly simplifies the canopy height estimation technique since the ground topography is as flat as the tidal range. SRTM data are distributed with a 90 m spatial resolution around the Earth, reduced from the original 30 m through averaging and subsampling. In a previous paper, Simard et al. (2006) used an airborne lidar (i.e. light detection and ranging) to calibrate SRTM elevation. Lidar measures the time of return of a light pulse reflected off a target and thus measures the relative distance. Recent results using space-borne lidar showed that these data could also be used to estimate vegetation height and correlate it with biomass (Lefsky et al., 2005; Drake et al., 2002a,b). GLAS (ICEsat Geoscience Laser Altimeter System) is the first space-borne lidar instrument for global observations of Earth (Schutz et al., 2005) which has been collecting data since early 2003 and is the benchmark Earth Observing System mission for measuring ice sheet mass balance, cloud and aerosol heights, as well as land topography and vegetation characteristics. Carabajal and Harding (2006) showed that the GLAS waveform (laser return as a function of time) centroid is highly correlated to the SRTM phase center elevation over densely vegetated regions.

In this paper, we present a methodology based on SRTM elevation, ICEsat/GLAS, and field data to map mangrove forest height and aboveground biomass. We focus on the Cienaga Grande de Santa Marta (CGSM), Colombia, a large wetland complex where one of the largest mangrove rehabilitation projects in Latin America is currently underway (Botero & Salzwedel, 1999; Rivera-Monroy et al., 2004; Rivera-Monroy et al., 2006). Large man-made hydrological modifications in the region caused hypersaline soil conditions (>90 g kg^{-1}) since the 1960s triggering a large dieback of mangrove wetlands (~247 km^2). Thus, remote sensing tools are needed to evaluate if current freshwater diversions initiated in 1995 will be successful in restoring mangrove wetlands at the landscape scale. Our objective is to build a baseline map to quantitatively estimate the extent, height and biomass of the mangrove forests in CGSM. We describe how to use ICEsat/GLAS data to systematically calibrate SRTM elevation data, potentially providing a robust method to extend 3D mapping of mangrove forests to other parts of the World. In addition, we collected field data on structural attributes along four mangrove transects in CGSM to calibrate SRTM and to derive a site-specific relationship between mean canopy height and aboveground biomass. The GLAS and field data do not overlap since we were unable to obtain accurate geolocation for our sampling points because of weak GPS signal under the dense canopy. We relied on distance and orientation using a measuring tape and a compass to locate the sampling points on the SRTM maps. The height–biomass relationship enables mapping of biomass in CGSM by extrapolating with the calibrated SRTM canopy height estimates. Biomass estimates in this ecoregion are badly needed to evaluate the impact of mangrove mortality on nutrient cycling (i.e. carbon, nitrogen, phosphorus) and to understand how the loss of above- and belowground biomass affect the role of mangroves as carbon sinks.

2. Data and methods

2.1. Site description

Located on the Caribbean coast (10° 37′ to 11° 07′N and 74° 15′ to 74° 51′W), the Ciénaga Grande de Santa Marta (CGSM) forms the exterior delta of the Magdalena River, the fifth largest river in South America with an annual average water discharge of 7000 m^3 s^{-1} (Restrepo & Kjerfve, 2000; Rivera-Monroy et al., 2004) (Fig. 1). The wetland complex was designated as a Wetland of International Importance under the Ramsar Convention by the Government of Colombia on the 18th of June 1998 (Ramsar site no. 951). It was also designated as a UNESCO Biosphere Reserve in 2000. The CGSM is the largest lagoon–delta complex in Colombia (1280 km^2). To the north, the ecosystem is separated from the Caribbean Sea by the barrier island Isla de Salamanca, which has an inlet (Boca de la Barra) approximately 100 m wide and 10 m deep on its eastern end that connects the largest lagoon directly to the sea. To the

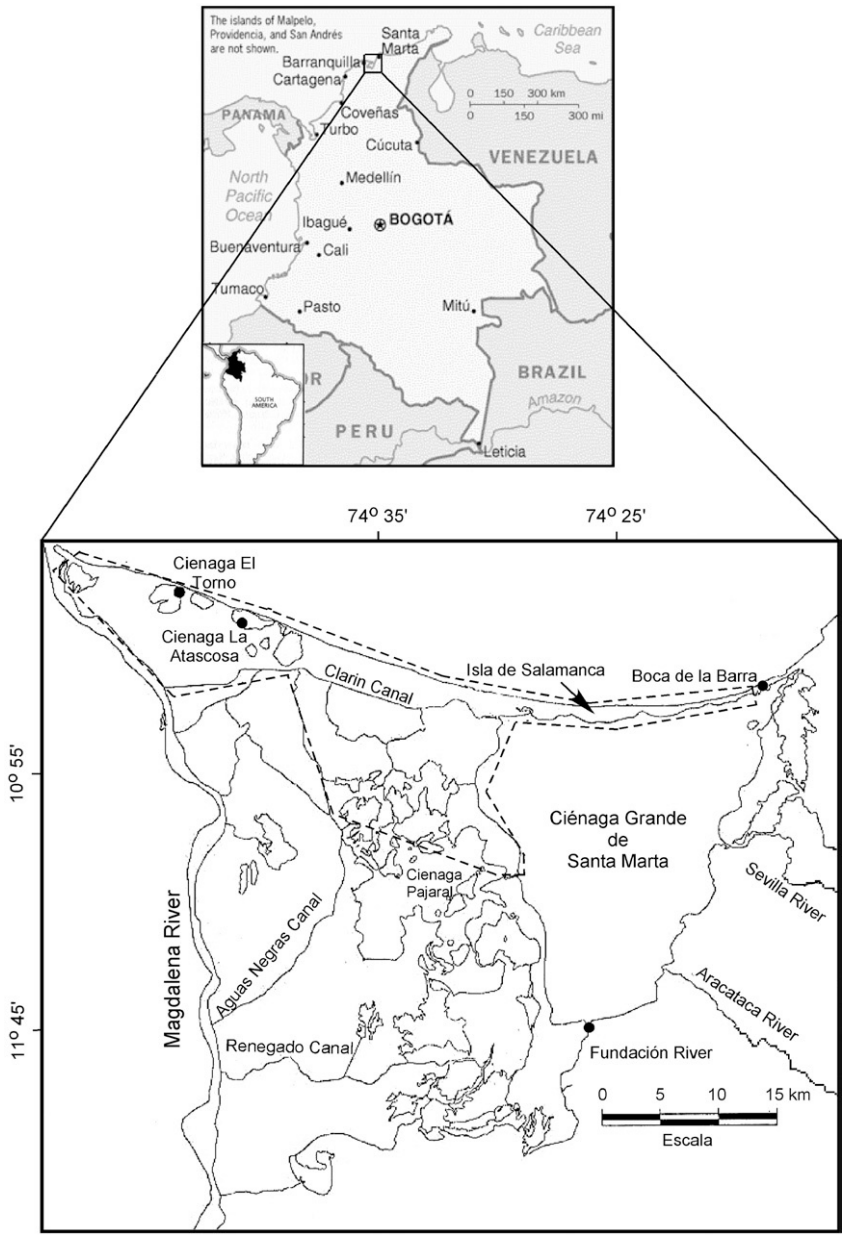

Fig. 1. Map of the Cienaga Grande de Santa Marta (CGSM) lagoon–delta complex with location of the field transects used to characterize structural attributes of mangroves. Transects were selected on each side of Boca Fundacion River (i.e. one on the east and one on the west of Fundacion River shown on the map), at Cienaga El Torno and Cienaga La Atascosa. The dotted area represents the boundary of the Salamanca National Park.

west and southwest the lagoon–delta complex is limited by the flood plain of the Magdalena River, through which five main tributaries historically brought freshwater from the river to the complex until the 1970s. To the east and southeast, CGSM is bordered by the foothills of the Sierra Nevada de Santa Marta, the highest coastal mountain in the world (5800 m above sea level). Four main rivers drain this watershed, crossing an extensive agricultural zone and draining into the major lagoon with an average annual flow of about 20 $m^3\ s^{-1}$ (Botero & Salzwedel, 1999; Rivera-Monroy et al., 2004). According to its geomorphological, geophysical and biological characteristics, CGSM can be classified as Type I setting (Thom, 1982), that is river-dominated with micro tidal regime (±30 cm), and arid climate (Twilley et al., 1998). The micro tidal regime implies ground topography in the mangrove forest to vary only within 30 cm. The estuarine regions were surrounded until around 1960 by approximately 52,000 ha of mangrove wetlands dominated by *Rhizophora mangle* (L.), *Avicennia germinans* (L.), and *Laguncularia racemosa* (Gaertn) (Cardona & Botero, 1998).

The CGSM was strongly impacted by human activities that disrupted major hydrological linkages at both freshwater and marine boundaries. The anthropogenic alterations started with a highway constructed in 1956 that interrupted most of the connections between the Caribbean Sea and the system. After 1970, fresh water from Magdalena River was diverted from CGSM by a road built along the river without culverts. This resulted in soil hypersalinization that caused the death of

Table 1
Proportion (percentage) of tree species tallied during the field campaign by sites and overall CGSM

	West of Fundación (5 plots)	East of Fundación (5 plots)	Torno (4 plots)	Atascosa (2 plots)	CGSM (16 plots)
R. mangle	8	10	42	89	28
A. germinans	92	88	40	0	66
L. racemosa	0	2	18	11	6

The overall CGSM percentages are computed using every tree from all plots. The number of plots is in parenthesis.

approximately 70% of the original mangrove forest. The rate of mangrove loss has gradually increased from 1.75 $km^2\ yr^{-1}$ from 1956 to 1968, to 9.8 $km^2\ yr^{-1}$ from 1968 to 1987, to 13.32 $km^2\ yr^{-1}$ from 1987 to 1993. The peak rate occurred from 1993 to 1995 at 18.43 $km^2\ yr^{-1}$ (Cardona & Botero, 1998; Gónima et al., 1998).

Hydrologic alterations have also caused water quality changes in the ecosystem, mainly in the Pajarales Complex. For the past four decades, the system has undergone severe environmental stress associated with fresh water diversion, causing large-scale mortality of mangroves (mainly in the Pajarales Complex, Fig. 1), fish kills, water contamination, and loss of biodiversity (Santos-Martínez & Acero, 1991; Mancera & Vidal, 1994; Botero & Mancera, 1996; Cardona & Botero, 1998). Since 1996, a large-scale rehabilitation project has been implemented in the system to restore the hydrologic regime and induce the natural regeneration of mangrove forests to improve water quality and local fisheries production (Twilley et al., 1998; Botero & Salzwedel, 1999; Polania et al., 2001).

The area serves as habitat and winter breeding ground for several bird species, and spawning ground for many fish species. CGSM has been the main source of fish and shellfish for the north coast of Colombia (Santos-Martinez & Acero, 1991; Mancera & Mendo 1996; Rueda & Santos-Martinez, 1999; Rueda, 2001). The ecological values of the system are well known, as it is already declared as two national protected areas: the Vía Parque Isla de Salamanca and the Santuario de Fauna y Flora de la Ciénaga Grande de Santa Marta. Part of the site is state-owned, while a large area is privately-owned and commercial and artisanal fishing is important for human communities living around the lagoon. Shellfish and crayfish are also harvested in the area, while higher elevation zones are used for agriculture. Ecotourism is also being developed in the protected area.

Table 2
Sample fits for each mangrove specie as shown in Fig. 2

Mangrove specie	Regression fit	Error in rms percent
R. mangle	$DBH = 1.2 * H$	0.3
A. germinans	$DBH = 1.1 * H + 0.05 * H^2$	0.52
L. racemosa	$DBH = 1.1 * H$	0.46

2.2. Field data

We collected field data in August 2005 along four mangrove transects in CGSM (16 plots): east and west side of Boca Fundación River and two transects (Ciénaga El Torno and Ciénaga La Atascosa) located in Vía Parque Isla de Salamanca (Fig. 1). We used the variable circular plot method (Grosenbaugh, 1952; Dilworth & Bell, 1975) to select trees. This method allows efficient sampling of large trees that generally have lower spatial density than smaller trees. In variable plot sampling, plot size is dependent on tree diameter, and trees are tallied as "in" or "out" of the plot depending on whether their diameter at breast height (DBH) is large enough to subtend a fixed critical angle visible using an angle gauge from the plot center. Each "in" tree accounts for a fixed basal area. Since the angle is known, we can also estimate the spatial density of trees as a function of DBH. Using a Basal Area Factor of 5 (0.0232 rad at arm length), we tallied a total of 166 trees, an average of 10 trees per plot. For each of the selected trees, we identified the species (Table 1), measured height

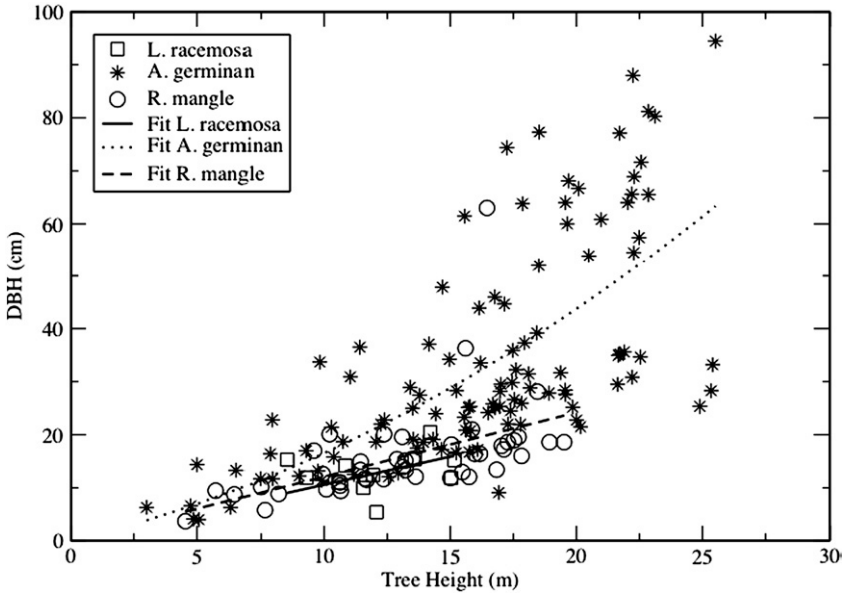

Fig. 2. Measured diameter at breast height (DBH) and tree height for each specie at all sites in CGSM. The fits are given in Table 2.

using a laser ranger, and measured DBH with a DBH tape. The data collected are shown in Fig. 2 and regression fits are given in Table 2. In the field, a tree height measurement by different operators varied significantly due the difficulty in identifying a specific tree top in a dense canopy. We found, by field experiments, that it caused a tree height measurement random error of approximately 10%. Geographical location was obtained where possible with a hand held GPS (Global Positioning System). The GPS coverage under the mangrove canopy was poor and insufficient to find the exact location of the ICEsat footprint. To complement the GPS data, we followed a straight line with a constant compass reading and measured the distance between plots in each transect with a metric tape. Based on the data, we estimated a maximum location error of 43 m.

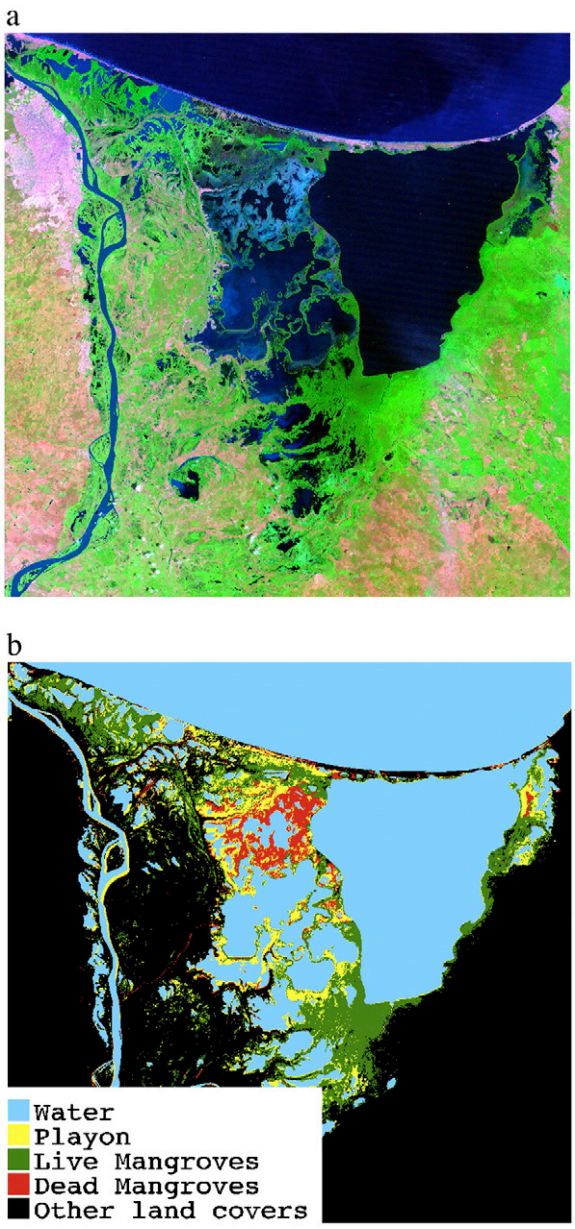

Fig. 3. a) Landsat 5 image of March 4th, 1999 in Red–Green–Blue color composite with bands 7, 4 and 1 respectively. The dark blue areas are water and the mangroves are in shades of green while the dead mangroves are seen in bright blue. The surrounding region is covered mainly by agriculture (orange and green colors), plantations (green color) and urban areas (pink color). The city of Barranquilla is on the Western side along the Magdalena River. b) Land cover classification showing live and dead mangrove forests produced from the 1999 Landsat 5 scene using Isodata algorithm. The confusion matrix is given in Table 3.

2.3. Land cover map

We produced a land cover map specific to the mangrove forests of CGSM using a cloud free Landsat 5 TM scene from March 1999 (Fig. 3a). The species composition of CGSM is generally mixed with a variety of proportions (Table 1) and the dominant species may change rapidly over tens of meter. Therefore, we use the Landsat scene to derive generic mangrove classes with a standard non-supervised IsoData classification algorithm (Iterative Self-Organizing Data Analysis; Jensen, 1996). This method is used instead of supervised algorithm because it does not require the interpreter to select training samples for every potential land cover in the image that would otherwise result in multi-modal class distributions. Isodata simply requires setting an arbitrary number of classes that are merged subsequently by the user. First, all areas with SRTM topography greater than 30 m were masked since there are no taller mangrove forests in CGSM and there cannot be mangroves outside the intertidal region at 0 m elevation. Isodata with 30 classes resulted in spatial patterns corresponding to those observed by visual interpretation. The 30 classes were then merged into a final four land cover classes by visual interpretation using field data and expert knowledge of the area. The four land cover classes are: *water*, *playon*, *live mangroves*, *dead mangroves* and *other*. The *playon* are usually mud flats that may have been partially covered with mangroves in the past. The *Dead Mangroves* class is characterized by forest remnants with dead trunks and branches. The *Live Mangroves* class is the generic class of mangrove forest with any mixture of the three species found in CGSM. Finally, all other land covers such as agricultural, urban, sand and bare soils, plantations etc. are included in class *Other Land Covers*. The final land cover map is shown in Fig. 3b.

The land cover classification had a 100% accuracy within the field transects locations and the perimeter of the Ciénaga lagoon (Fig. 1) which is bordered by live and dead mangroves areas. Due to the limited field sampling, we obtained an estimate of the classification accuracy by selecting validation samples again by visual interpretation of the Landsat scene, field data, *Google*

Table 3
Confusion matrix in percent for land cover map of Fig. 3b

Class	Water	Dead	Other LC	Playon	Mangroves
Water	*99.95*	0	0	7.38	0.04
Dead mangroves	0	*98.54*	0	11.66	0
Other classes	0	0	*99.05*	0.	14.85
Playon	0.05	1.2	0.08	*69.73*	0.02
Live mangroves	0	0.27	0.87	11.22	*85.08*
Total	100	100	100	100	100

Earth images, and knowledge of the region. We obtained a confusion matrix (Table 3) with an overall classification accuracy of 80%. The *live mangrove* class covers 29,042 ha with an estimated 4 and 15% commission and omission error respectively. The *dead mangroves* class covers 7431 ha and the *playon* class 19,683 ha with errors shown in Table 2.

2.4. Shuttle Radar Topography Mission (SRTM) data

In February of 2000, Space Shuttle Endeavour collected nearly global coverage of Earth's topography using radar interferometry (SRTM, Shuttle Radar Topography Mission). Because of limited penetration of microwaves within vegetation, the SRTM topographic maps contain information related to vegetation height (Kellndorfer et al., 2004). The SRTM C-band data are distributed freely at a spatial resolution of 30 m over the U.S. and 90 m for the rest of the World (Slater et al., 2006). Therefore, the SRTM elevation data has a 90 m spatial resolution in CGSM. We used SRTM's Version 2 data (by naming convention SRTM3 for 3 arc sec data) from the Jet Propulsion Laboratory. These data were built by box averaging with a window of 3 by 3 elevation pixels.

2.5. GLAS waveforms

Laser pulses from ICEsat/GLAS illuminate spots (footprints) about 70 m in diameter and spaced at about 172 m intervals along Earth's surface. GLAS records the energy return as a function of time (i.e. lidar waveforms). GLAS waveforms are characterized by a single Gaussian peak over oceans, sea ice, and ice sheets, however multiple peaks may occur over irregular surface such as land covered by vegetation. As described by Brenner et al. (2003), the return signal can be represented as a sum of Gaussian peaks plus a bias. For land surfaces, the ICEsat/GLAS standard algorithm characterizes the return pulse by using multiple Gaussian distributions to fit every mode (peak) in the waveform (Harding & Carabajal, 2005). The standard ICEsat elevation product over land (i.e. GLA 14) is derived from the centroid of the return (Brenner et al., 2003). Since the CGSM is relatively small, we were able to collect all waveforms (i.e. product GLA 01) located in this area and perform data processing to estimate tree height.

The use of ICEsat/GLAS waveforms to characterize mangrove forests is a new and systematic approach to improve mapping accuracy of mangrove canopy height by calibrating SRTM elevation data. We used GLAS waveforms to estimate mangrove forest height where data over mangrove forests were available. As of October 2006, we found a total of 326 ICEsat/GLAS footprints located in mangrove forests of CGSM after we eliminated the waveforms with low signal voltage and high thermal noise (i.e. maximum less than 0.3 V or mean thermal noise greater then 0.1 V as estimated from the beginning of waveform). Most footprints are located on the Eastern side of Boca Fundación and Parque Isla de Salamanca. In the case of mangrove forests, the GLAS waveforms are generally bimodal distributions resulting from scattering within the canopy and the ground. The top of the canopy in a mature mangrove forest is homogeneous and is generally void of understory vegetation with roots and detritus on the ground, while the scrub mangrove canopies are short and dense vertically. Thus a *clean* bimodal waveform can be expected for tall mangrove forests but not for scrub mangroves. Generally, the waveforms from Boca Fundación GLAS transects have a significant contribution from a secondary lower canopy (i.e. Gaussian peaks between the ground and the main canopy) suggesting canopies with irregular surfaces while the Salamanca transects are dominated by the tall canopy signature.

3. Analysis and results

3.1. Mangrove extent in CGSM

The total estimated mangrove forests extent using the 1999 land cover map was 29,042 ha (Fig. 3b) with an estimated 4% and 15% commission and omission error respectively (Table 3). This is less than half the value reported by Cardona and Botero (1998) before 1960 and higher than values reported for 1995 (16,631.48 ha) before the diversion of freshwater as part of the rehabilitation project (Twilley et al., 1998; Gónima et al., 1998). In the land cover map, the dead mangrove class accounts for an extra 7431 ha located in the hypersaline soils (Pajarales complex, Fig. 1) clearly distinguishable in the remote sensing imagery (Fig. 3a). This class sets a minimum value on mangrove area loss since the early 1960s. In addition, the *playon* class may have been partially covered with mangroves several decades ago; if the *playon* is accounted for, the area loss is 27,114 ha. The total area covered by these three classes (56,156 ha) is similar to the 1960s 52,000 ha of mangrove area (Cardona & Botero, 1998).

3.2. Estimation of mangrove forests height from field data

In this section, we describe the methodology used to compute the mangrove canopy height from the field data. Fig. 2 shows the large natural variability found within the mangrove forest. Since our sample sets are relatively small (an average of 10 trees per plot), it is important to consider the impact of this variability on extrapolations necessary to calibrate a 90 m SRTM pixel. *A. germinans* is the dominant specie in CGSM with a height variability for a given DBH of 52% (Table 2). Historically, *A. germinans* was the dominant species in this semi-arid coastal region due to its physiological adaptations to withstand high soil salinities (Rivera-Monroy et al., 2001). For *A. germinans*, our sampling set has an average DBH and height of 33.4 cm and 16.1 m respectively. Given the angle gauge of 0.0232 rad, this DBH represents an "in" tree with a maximum plot radius of 14.4 m. To estimate tree spatial density (trees/ha) of this DBH population (i.e. 33.4 cm), we multiply by 15.35, obtained from the ratio of plot sizes 1 ha/($\pi 14.4^2$), and the canopy height means are computed on the extrapolated samples, thus preserving the sample error. The plot sizes are significantly smaller than SRTM spatial resolution and it is reasonable to assume that the natural height variability observed in Fig. 2 was not fully represented within our plot.

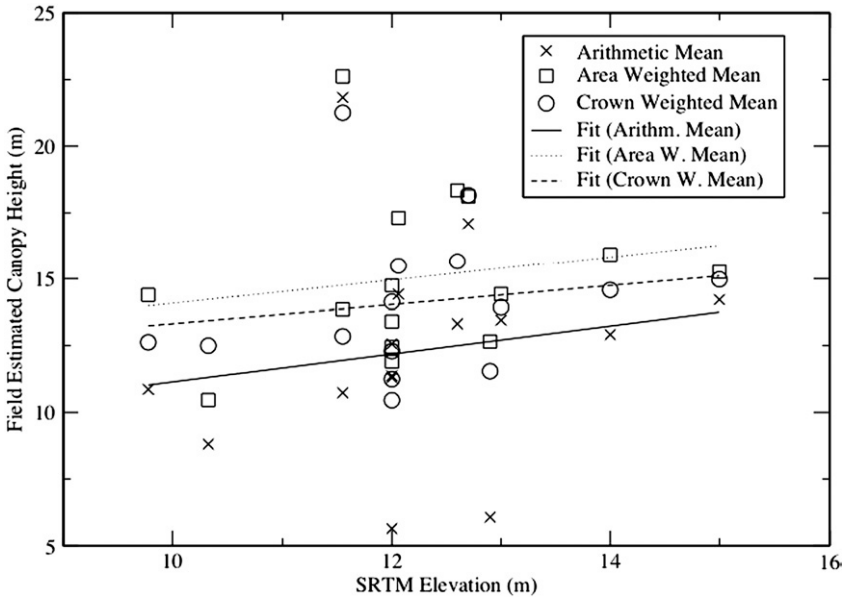

Fig. 4. Field estimates of forest height compared to SRTM elevation within the four sampling sites shown in Fig. 1. The variability of the height estimator with respect to SRTM elevation is given in Table 4. The fits were uncorrelated and therefore are not used in the study.

Therefore, assuming that the impact of this variability (i.e. 52% with DBH) is random, the mean canopy height estimation has an error of 2.6 m ($16.1 \cdot 0.52/\sqrt{10}$). Including the normalized height measurement error in the field ($\sqrt{\left((16.1 \cdot 0.1)^2+(16.1 \cdot 0.52)^2\right)/10}$), we obtain a field canopy height estimation error of approximately 2.7 m.

We investigated several methods to compute the mean canopy height from the field data: the *arithmetic mean*, the *coverage area weighted mean* and a *crown weighted mean*. The *arithmetic mean* does not take into account crown size of trees although it varies significantly with tree height and size and thus considers small trees occupy as much horizontal space as large trees. On the other hand, we used two canopy height estimates based on a weighted mean, adjusting the aerial coverage of a single tree to its height, i.e. the taller the tree the wider the crown:

- The *coverage weighted mean* uses a simple linear relation between tree height and crown coverage area assuming that the canopy is closed. Thus, the sum of the weights of all trees within the plot is equal to the area A of the plot and the canopy is completely closed (100% cover). For example, if there are n trees in a plot of size A, the mean area occupied by a tree is $x=A/n$ with a radius $r=\sqrt{x/\pi}$. If the mean tree height of the plot is H, then r/H can be used as the slope to compute the area a occupied by each tree of height h in this plot such that $a=\pi(r/H*h)^2$;
- The *crown weighted mean* is based on an empirical relation between tree DBH and crown diameter $r=0.222*\mathrm{DBH}^{0.654}$ (Cintron & Shaeffer-Novelli, 1984). The weight is defined as the area of the crown (i.e. circular disk) and is not related to the plot area. Thus this height estimate is more realistic when the canopy is not completely closed.

The regression fits shown on Fig. 4 had poor correlation (below 0.2) and cannot be used for calibration. Instead, we used the field data means to estimate the random error (rms) and SRTM bias which results from microwave penetration within the canopy and residual miscalibration of *SRTM3*. The rms variation and biases between SRTM elevation and field data means are given in Table 4. As expected, the arithmetic mean is generally lower than the weighted means since large trees (DBH) have larger crowns and weigh more in the computation of the mean height. The crown weighted mean is the most consistent with SRTM elevation with an overall rms noise of 2.9 m but generally less than 1.8 m, except for the transect East of Boca Fundación. The large variation within this site is mainly due to a single plot clearly visible above 20 m in Fig. 4. It is apparently an outlier that when removed, reduces the overall bias and rms variation to -1.3 ± 1.9 m. The plot may have been part of an isolated patch (~30 m in width) of taller trees whose height signature is smoothed or removed in the 90 m SRTM

Table 4
This table compares the mean canopy height estimations from field data and SRTM elevation

Field height method	East of Fundación	West of Fundación	Torno	Atascosa	Overall
Arithm. mean (m)	−2.8±3.5	3.0±3.1	0.3±0.6	0.2±0.6	0.0±3.9
Crown weight (m)	−3.8±2.7	−0.5±1.8	−0.6±1.2	−0.5±0.5	−1.7±2.9
Area weight (m)	−4.9±2.5	−1.4±1.8	−1.4±1.2	−0.8±0.6	−2.6±3.0

The first value is a mean canopy height bias ($H_{\mathrm{bias}}=H_{\mathrm{SRTM}}-H_{\mathrm{field}}$) and the second is the SRTM rms height error (i.e. ±rms). Overall, the *crown weighted mean* is the field height estimation method most similar to the SRTM elevation with an rms of 2.9 m.

elevation data product. Neglecting this plot, we obtain the following correction for SRTM bias:

$$H_{\text{field}}(\pm 1.9\ \text{m}) = 1.3 + H_{\text{SRTM}}. \quad (1)$$

3.3. Estimation of mangrove forest height with ICEsat/GLAS waveforms

The ICEsat/GLAS waveforms can be used to quantitatively characterize canopy structure and model the Canopy Height Profile (CHP) as the relative distribution of canopy surface area (Harding et al., 2001). To derive the CHP from the lidar waveform, one must consider light occlusion resulting from interception of light from upper layers. Light occlusion reduces the signal contribution from lower layers of the canopy. The technique is based on several assumptions such as a random distribution of horizontal canopy components independent of layers above and below, a constant leaf orientation, and reflectivity as a function of height also implying the ratio of wood and leave material is constant as a function of height. First the waveform ground component is scaled to account for difference in reflectivity (50%) within the canopy. Then, canopy closure is modeled by computing the cumulative distribution of the waveform from the top to the bottom of the canopy and normalized by the total return of the canopy and ground. This height distribution of canopy closure is then weighted by an

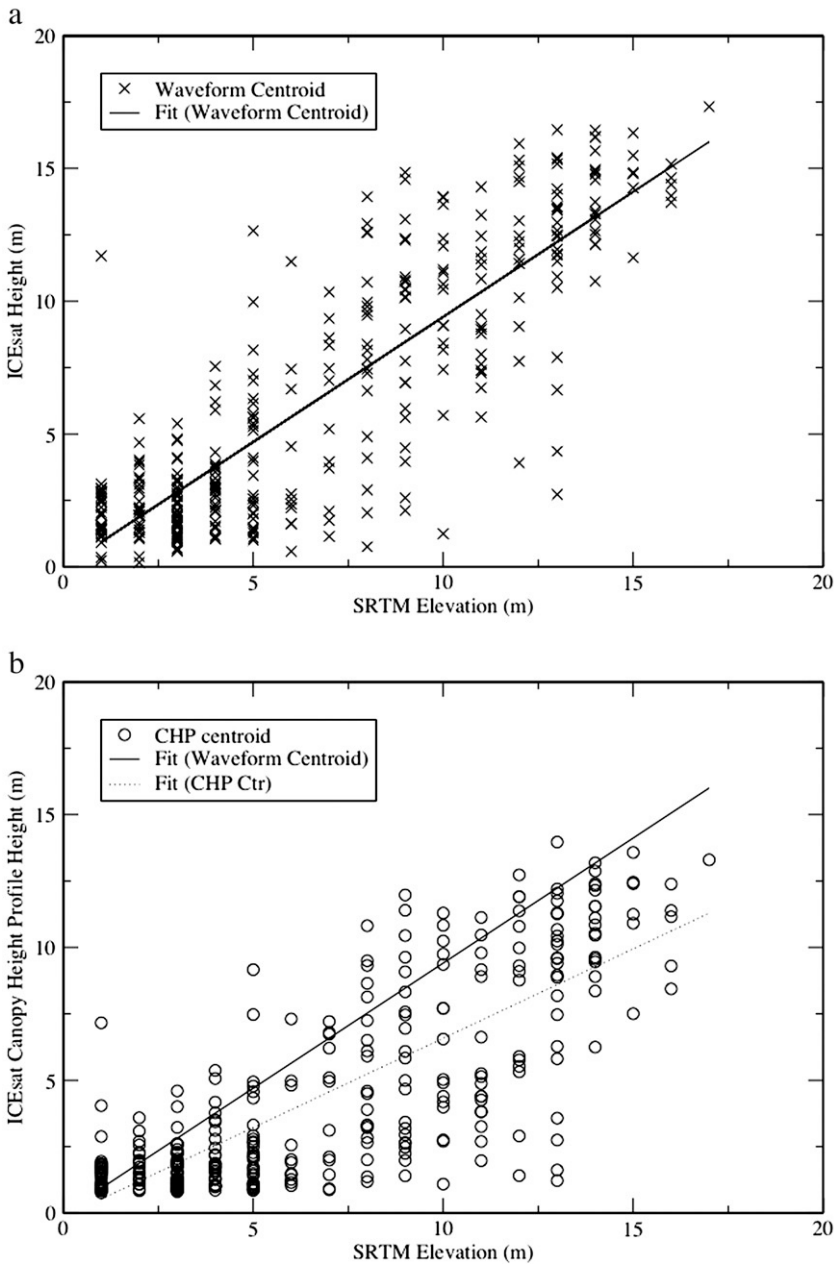

Fig. 5. Relation between a) canopy height estimation from ICEsat/GLAS Canopy Waveform Contribution (CWC) and SRTM elevation and; b) canopy height estimation from ICEsat/GLAS Canopy Height Profile (CHP) and SRTM elevation. As a reference the linear fit of the CWC estimates is also shown in (b).

occlusion transformation of the form [−ln(1−closure)]. It is finally normalized to obtain a cumulative distribution of plant area. In summary, the CHP transform should increase the signal level of the lower layers of the canopy in the waveform as if all layers received an equivalent amount of light. Although, we do not have sufficient data to realistically validate the CHP, we perform our analysis on both raw waveforms and CHP's as described by Harding et al. (2001).

The overall analysis includes characterizing the canopy and ground contributions within the waveform. We began by fitting a single Gaussian distribution to the GLAS recorded transmitted pulse (a copy of the laser pulse transmitted by the lidar instrument is recorded by the GLAS system). This fit is then matched to the waveform ground peak to accurately determine the ground location within the waveform. Then we estimated the thermal noise level (system and measurement noise) using the data between the beginning of the waveform and the top of the canopy. In order to locate the top of the canopy (i.e. maximum height) within the waveform, we found that using the maximum noise value was more robust than the rms noise level for batch processing. We defined the top of the canopy as the first waveform sample with a voltage value larger than twice the maximum thermal noise value. Finally, Gaussian distributions were fitted to the remaining of the waveform until the rms deviation of the fit converged below the thermal noise level. At this point the remaining variations are due to noise and not to forest canopy signal.

The waveform centroid is computed on the multiple Gaussian fit in two ways: using the full waveform including the ground and canopy peaks and the waveform without the ground peak. The former closely corresponds to the standard GLAS algorithm (Harding & Carabajal, 2005) to estimate ground elevation while the latter is designed to extract the Canopy Waveform Contribution (CWC). The CWC is obtained by subtracting the recorded transmitted pulse from the waveform at the detected ground peak position and computing the centroid of the remaining signal. Thus CWC is an estimate of the canopy height.

The combined georeferencing error of ICEsat (2.4 m error) and SRTM (9 m error for South America) is 9.5 m. The geolocation error and the different spatial resolution and sampling lead to different portions of the forest being sampled. Fig. 5 shows the comparison between height estimates from ICEsat CWC and CHP models with SRTM elevation data (i.e. *SRTM3*). The resulting linear fits are the following:

$$H_{\mathrm{CWC}}(\pm 2.6\ \mathrm{m}) = 0 + 0.94\ H_{\mathrm{SRTM}} \quad (2)$$

$$H_{\mathrm{CHP}}(\pm 2.3\ \mathrm{m}) = -0.1 + 0.67\ H_{\mathrm{SRTM}}. \quad (3)$$

In both cases the intercept and slope errors are 0.2 and 0.03 with correlations of fits 0.85 and 0.8 respectively. As expected, the impact of the CHP transform is to lower the canopy height estimate; the smaller slope of Eq. (3) indicates the higher the SRTM elevation, the more it is reduced as compared to CWC. The estimation of height using CHP does not agree with the field data; using the average field plot height of 13.6 m as a reference, Eq. (2) implies SRTM elevation should be 20.4 m. The mangrove forests generally have sparse understory, and light occlusion occurs within a tree crown not obstructing light penetration to neighboring smaller trees (e.g. small trees populating gaps). Thus, we assume that most of the energy is reflected from the top layers of the canopy and the ground, especially when there are canopy gaps. In summary, neglecting light occlusion and using CWC means that we are in fact describing the height distribution of the *canopy surface*. This assumption is also supported by the similarity between the CWC estimates and SRTM elevation (Fig. 5a). The similarity between the measurements indicates that radar scattering in mangrove forests occurs mainly in the upper canopy. These results are similar to findings in Everglades National Park (Simard et al., 2006) and other types of vegetation (Carabajal & Harding, 2006).

The rms variation between SRTM elevation and GLAS CWC is 2.6 m, which is significantly lower than observed for other types of forests (Carabajal & Harding, 2006) and close to the SRTM elevation random error reported for flat areas by Rodriguez et al. (2006). The difference between SRTM and ICEsat/GLAS is due to different parts of forest sampled, natural variability, differences in electromagnetic scattering mechanisms, system noise and a potential *SRTM3* calibration bias. We found a positive bias value of 1±1 m in bare ground areas near mangrove areas of CGSM.

Finally, we also searched for a potential correlation between height estimation error and canopy closure using the ratios of the waveform components for canopy and total return (Harding et al., 2001). We found that most waveforms in CGSM (i.e. 69% of the waveforms) were dominated by the canopy component (ratio >0.5) and found no correlation between canopy closure and height estimation error.

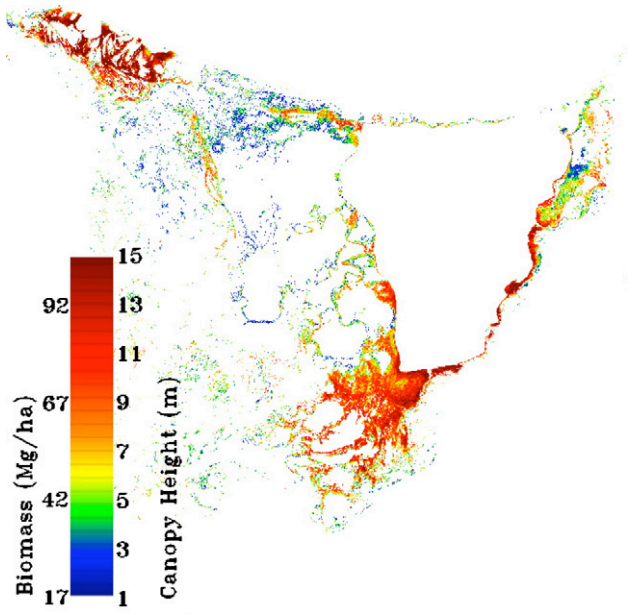

Fig. 6. Map of height and biomass of live mangrove forest built from SRTM elevation data.

3.4. Calibrating SRTM mangrove height estimation

ICEsat provides a systematic method to calibrate SRTM data wherever field data is not available with accurate geolocation and a large (~70 m) footprint close to *SRTM3*'s spatial resolution (~90 m). We removed the residual SRTM bias by combining the field data bias and ICEsat calibration (Eq. (2)). The average field plot height was 13.6 m with an overall SRTM height bias of −1.3 m. The relation between ICEsat waveform centroid height and SRTM elevation (Eq. (2)) indicates that SRTM elevation should be 14.5 m to obtain the calibrated 13.6 m. Thus the impact of calibrating SRTM with ICEsat is to reduce SRTM elevation values and thus the resulting bias to −2.1 m, which is still within the error margin of the field data (i.e. −1.3±1.9 m). The final calibration equation using both field and ICEsat height estimates becomes:

$$H_{\mathrm{CWM}}(\pm 1.9\ \mathrm{m}) = 2.1 + 0.94\ H_{\mathrm{SRTM}}, \quad (4)$$

where H_{CWM} is the *crown weighted mean height* of the mangrove forest canopy and H_{SRTM} is the SRTM elevation. This equation is the mean height of the *canopy surface* since radar and lidar penetration through the canopy were corrected

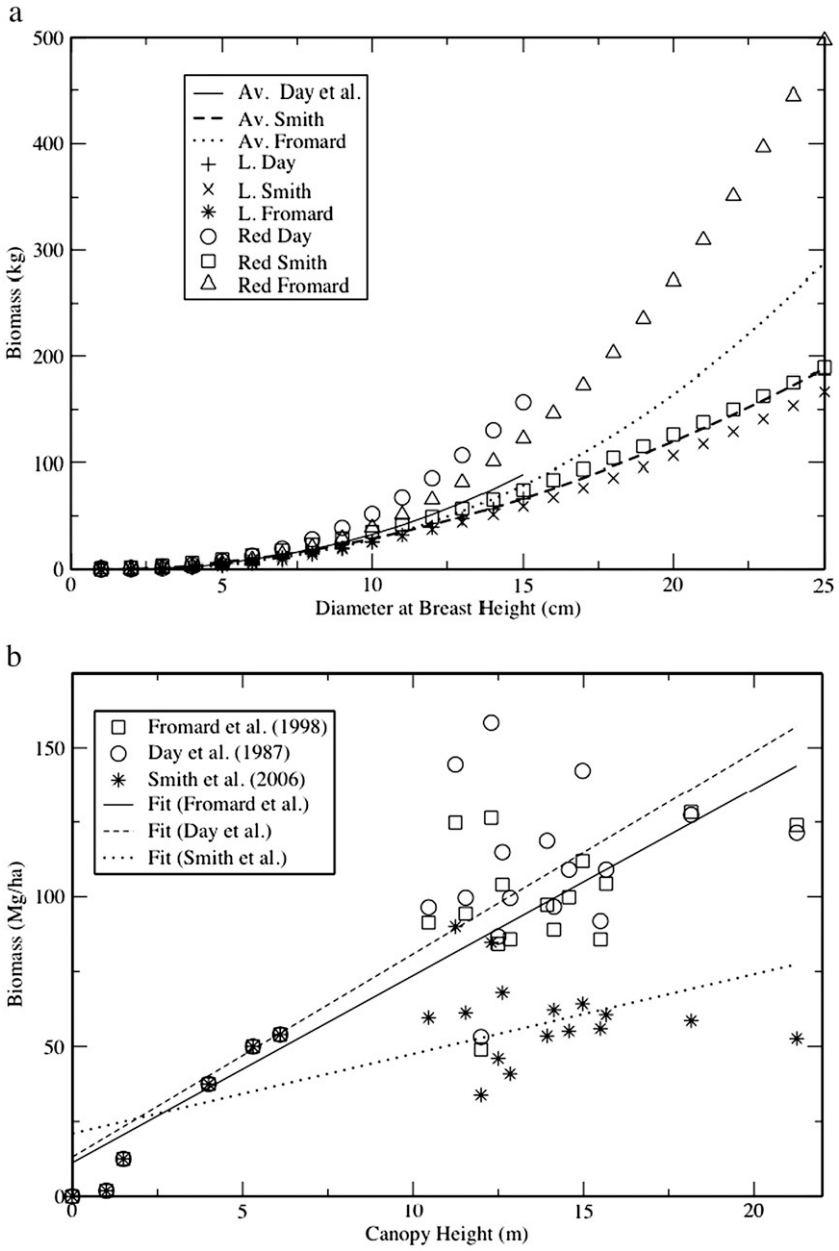

Fig. 7. a) Comparison of the three sets of allometric equations used in this study. These equations are for single trees of the three species found in CGSM: *A. germinans* (Av.), *L. racemosa* (L) and *R. mangle* (red). While the equations of Day et al. (1987) may not be applicable to trees larger than 15 cm, there is also a large discrepancy between the equations of Smith and Whelan (2006) and Fromard et al. (1998) reaching about 200 kg for a *Rhizophora mangle* tree of 25 cm DBH. b) Estimation of biomass as a function of plot mean tree height weighted by crown size. The slopes and error obtained for each allometric equations are given in Table 5.

Table 5
Height–biomass relation: B (Mg/ha)=m*Height (m)

Allometric equations	Regression fit b_0+m*H_{CWM}	Intercept error	Slope error	Correlation of fit	Residual RMS
Fromard et al.	$B=11+6.2H_{CWM}$	9	0.7	0.9	18.6
Day et al.	$B=13+6.8H_{CWM}$	12	1.0	0.84	25.5
Smith and Whelan	$B=21+2.7H_{CWM}$	8.2	0.7	0.67	17.3

The correlation and the rms residual error indicate the goodness of the linear fit and the residual variability of the data respectively.

by using the field data bias. Application of Eq. (4) to the *SRTM3* produces the calibrated mangrove forest height for the entire CGSM as shown in Fig. 6.

4. Estimation of biomass distribution and loss in CGSM

4.1. Allometric equations

We estimated aboveground biomass (B) of mangrove forests of CGSM as a function of mean canopy height using field data and published allometric equations (Fig. 7a). We chose the *crown weighted mean* to derive the biomass–height relationship since it is the canopy height estimator with the lowest rms difference with respect to SRTM canopy height measurement. We compared three different sets of allometric equations derived in Laguna de Terminos, Mexico (Day et al., 1987) French Guyana (Fromard et al., 1998) and the Everglades, Florida (Smith & Whelan, 2006). The first two sites have similar geomorphological settings (deltaic) and have large extension of mangrove forests as in the case of the CGSM. The third set was derived using trees from three locations within the Everglades National Park, a karstic dominated ecosystem. We only used the Day et al. (1987) equations for comparison purposes since they were derived from trees smaller than 15 cm DBH (Fig. 7a). We applied a linear regression through the field data (Fig. 7b) such that aboveground biomass (Mg/ha)=b_0+m*H_{CWM} (meters). The intercepts b_0 and slopes m for each allometric equation are given in Table 5. These slopes are lower than the value of $m=10$ estimated in the ENP (Simard et al., 2006) indicating that a forest of the same height contains less biomass in CGSM than in ENP.

To compute the spatial distribution of biomass at the landscape scale, we used the calibrated SRTM canopy height estimate H_{CWM} computed with Eq. (4). Fig. 8 shows the histogram distribution of canopy height in CGSM with a mean of 7.7 m. To assess potential variation in biomass estimates due to allometric equations, we used the models of Smith and Whelan (2006) and Fromard et al. (1998). Since each model represents different geomorphological settings, the calculated biomass ranges represent different environmental conditions influencing maximum asymptotic tree heights for each species (sensu). The resulting aboveground biomass distribution map is shown in Fig. 6 and the total biomass estimates vary between 1.2 and 1.7 (± 0.1)$\times 10^6$ Mg using Smith and Whelan (2006) and Fromard et al. (1998). Certainly, mangrove total biomass values are a relatively minor contribution to the regional carbon cycle. However, estimated

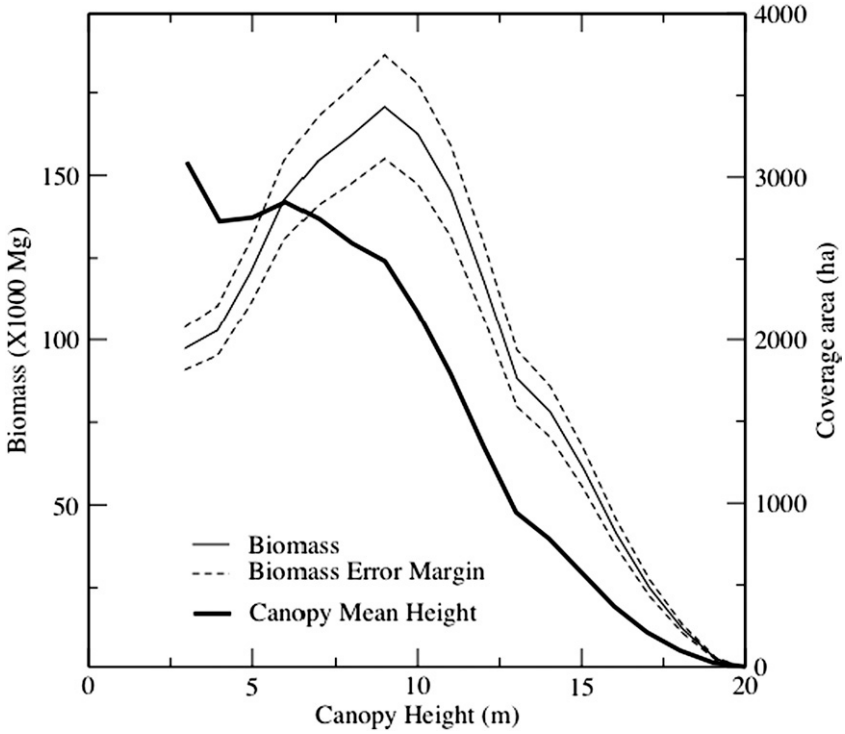

Fig. 8. Mangrove height and biomass distribution in CGSM. The mean forest canopy height weighted by crown size is 7.7 m. The biomass concentration peaks in 9 m forests.

values show that allometric equations are a critical component of robust biomass estimations and more efforts are necessary in deriving site-specific relations for carbon budgets and long-term monitoring of wetlands in the CGSM. In the context of the CGSM mangrove rehabilitation project, research efforts should be directed to estimating *in situ* allometric equations to improve present biomass estimates. These biomass values are first-rate estimates that illustrate the ecological application of tree height obtained through SRTM elevation and GLAS waveforms.

4.2. Biomass loss

Since we have estimates of area loss of mangrove forests as well as current biomass regression curves (Fig. 7b), it is possible to evaluate mangrove forest loss in terms of biomass. We assume that the dead forest had the same mean canopy height as the current forest with a mean aboveground biomass of 59 Mg ha^{-1} using the equations of Fromard et al. (1998). The estimated biomass loss is around 1.6×10^6 Mg considering an area loss of 27,114 ha. These biomass estimates will be used to evaluate the impact of mangrove mortality on carbon and nutrient cycling in the ecoregion. It is not clear how mangrove mortality has affected carbon cycling and how net export of dissolved organic and inorganic carbon and nutrients (nitrogen and phosphorus) from dead mangroves have modified water column productivity in open estuarine and coastal waters. Although there is a well-documented direct relationship between mangrove mortality and collapse of commercial and artisanal fisheries in the CGSM (Rivera-Monroy et al., 2006), it is not clear if mangrove impacted areas are contributing to increasing eutrophication as result of excess nutrient leaching from dead mangrove forests.

5. Conclusion

We presented a method using ICEsat/GLAS, SRTM and field data to estimate height and biomass distribution in the Ciénaga Grande de Santa Marta (CGSM), Colombia. ICEsat/GLAS data does not provide a complete and spatially continuous picture of the CGSM but is a powerful tool to estimate canopy height profiles (CHP) and canopy height. In this study, the extrapolation to large scale is achieved with SRTM elevation data, which contains a vegetation height signature due to limited microwave penetration in the canopy. Since SRTM data was acquired in February of 2000, the final maps represent the three-dimensional status of mangroves of that period. The mean mangrove canopy height in CGSM is 7.7 m and most of the biomass is concentrated in forest around 9 m in height (Fig. 8). We also found that CGSM may have lost approximately 27,114 ha of mangrove forests during the last decades.

Although the mangrove coverage around the world is relatively small compared to other ecosystems, the area may not reflect the ecological productivity and economical importance at regional levels, particularly in developing nations. The interest in deriving biomass estimates is due to the lack of data on this important ecosystem component at regional levels. Although global biomass estimates are not new for mangrove forests (e.g. Saenger & Snedaker, 1993), our results offer valuable information that can be readily used to produce regional estimates of carbon sequestration at tropical latitudes. And by providing a biomass budget, we demonstrate the direct utility of our method to evaluate ecosystem health as it is of great concern in the ongoing rehabilitation project in CGSM. We used different mangrove species-specific allometric equations to account for measurement and natural variability.

The biomass maps produced in this study are first order-estimates that will allow managers and scientists to evaluate regeneration rates of mangrove forest under hydrological rehabilitation at large spatial scales over the next decades, as well as to assess how highly disturbed mangrove forests respond to increasing sea level rise under current global climate change scenarios. The methodology could potentially be applied to any mangrove forests as long as ICEsat data are available and forest extent is sufficiently large to be mapped with the 90 m resolution SRTM data. The newest component from this study is the estimation of local values, with their respective accuracy, to produce data that can be used in other ecological studies (e.g. nutrient cycling) and to assess mangrove restoration/rehabilitation projects using "performance measures", such as biomass and tree height at landscape levels.

Acknowledgments

This study was conducted by the Jet Propulsion Laboratory, California Institute of Technology, under contract with the National Aeronautics and Space Administration (NASA) and funded by the NASA Interdisciplinary Science (IDS) program. This work was partially funded by the Instituto Colombiano para el Desarrollo de la Ciencia y la Tecnologia (COLCIENCIAS: code#: 2105-13-080-97) and the Instituto de Investigaciones Marinas (INVEMAR). We also acknowledge the support of the Instituto de Investigaciones Tropicales (INTROPIC) de la Universidad del Magdalena. We want to thank Paola Reyes Forero from INVEMAR and Alina Gamez Castro, Juan M. Carvajalino Fernandez, Maria Paz Consuegra, Fredy Guardiola, Yesenia R. Guerrero Belloso, Fatima C. Botto Lubo, Ivan Medina, Linda J. Ortiz Prada, Johan Rodriguez and Cesar Valverde from the Universidad del Magdalena and Eduardo Montero for field support and assistance.

References

Alongi, D. M. (2002). Present state and future of the world's mangrove forests. *Environmental Conservation*, *29*(3), 331−349.

Botero, L., & Mancera, J. E. (1996). Síntesis de los cambios de orígen antrópico ocurridos en los últimos 40 años en la Ciénaga Grande de Santa Marta (Colombia). *Revista de la Academia Colombiana de Ciencias*, *20*, 465−474.

Botero, L., & Salzwedel, H. (1999). Rehabilitation of the Cienaga Grande de Santa Marta, a mangrove–estuarine system in the Caribbean coast of Colombia. *Ocean and Coastal Management*, *42*, 243−256.

Brenner, A. C., Bentley, C. R., Csatho, B. M., Harding, D. J., Hofton, M. A., Minster, J., Roberts, L., Saba, J. L., Schutz, R., Thomas, R. H., Yi, D., & Zwally, H. J. (2003). *Derivation of range and range distributions from laser pulse waveform analysis for surface elevations, roughness, slope, and vegetation heights.* Algorithm theoretical basis document. Version 3.0 Greenbelt, MD: Goddard Space Flight Center.

Carabajal, C. C., & Harding, D. J. (2006). SRTM C-band and ICEsat laser altimetry elevation comparisons as a function of tree cover and relief. *Photogrammetric Engineering and Remote Sensing*, *72*(3), 287−298.

Cardona, P., & Botero, L. (1998). Soil characteristics and vegetation structure in a heavily deteriorated mangrove forest in the Caribbean Coast of Colombia. *Biotropica*, *30*, 24−34.

Cintron, G., & Schaeffer-Novelli, Y. (1984). Methods for studying mangrove structure. In S. C. Sneadaker & J.G. Sneadaker (Eds.), *The mangrove ecosystem: Research methods* (pp. 3−17). Paris: UNESCO.

Day, J. W., Jr., Conner, W. H., Ley-Lou, F., Day, R. H., & Machado Navarro, A. (1987). The productivity and composition of mangrove forests, Laguna de Terminos, Mexico. *Aquatic Botany*, *27*, 267−284.

Dilworth, J. R., & Bell, J. F. (1975). Variable plot cruising. In J. R. Dilworth (Ed.), *Log scaling and timber cruising* Corvallis, OR: Oregon State University Book Store, Inc.

Drake, J. B., Dubayah, R. O., Knox, R. G., Clark, D. B., & Blair, J. B. (2002). Sensitivity of large-footprint lidar to canopy structure and biomass in a neotropical rainforest. *Remote Sensing of Environment*, *8V.1*(2-3), 378−392.

Drake, J. B., Dubayah, R. O., Clark, D. B., Knox, R. G., Blair, J. B., Hofton, M. A., Chazdon, R. L., Weishampel, J. F., & Prince, S. D. (2002). Estimation of tropical forest structural characteristics using large-footprint lidar. *Remote Sensing of Environment*, *79*, 305−319.

Ewel, K. C., Twilley, R. R., & Ong, J. E. (1998). Different kinds of mangrove forests provide different goods and services. *Global Ecology and Biogeography Letters*, *7*, 83−94.

Fromard, F., Puig, H., Mougin, E., Marty, G., Betoulle, J. L., & Cadamuro, L. (1998). Structure, above-ground biomass and dynamics of mangrove ecosystems: New data from French Guyana. *Oecologia*, *115*, 39−53.

Gónima, L., Mancera, J. E., & Botero, L. (1998). Aplicación de imágenes de satélite al diagnóstico ambiental de un complejo lagunar estuarino tropical: Ciénaga Grande de Santa Marta, Caribe colombiano. *Serie publicaciones especiales del Instituto de Investigaciones Marinas y Costeras, INVEMAR. 4, Santa Marta* 56p.

Grosenbaugh, L. (1952). Plotless timber estimates — New, fast, and easy. *Journal of Forestry*, *50*, 32−37.

Harding, D. J., & Carabajal, C. C. (2005). ICESat waveform measurements of within-footprint topographic relief and vegetation vertical structure. *Geophysical Research Letters*, *32*, L21S10. doi:10.1029/2005GL023471

Harding, D. J., Lefsky, M. A., Parker, G. G., & Blair, J. B. (2001). Laser altimeter canopy height profiles: Methods and validation for deciduous, broadleaf forests. *Remote Sensing of Environment*, *76*(3), 283−297.

Held, A., Ticehurst, C., Lymburner, L., & Williams, N. (2003). High resolution mapping of tropical mangrove ecosystems using hyperspectral and radar remote sensing. *International Journal of Remote Sensing*, *24*(13), 2739−2759.

Jennerjahn, T. C., & Ittekkot, V. (2002). Relevance of mangroves for the production and deposition of organic matter along tropical continental margins. *Naturwissenschaften*, *89*, 23−30.

Jensen, J. R. (1996). *Introductory digital image processing — A remote sensing perspective.* : Prentice-Hall.

Kathiresan, K., & Rajendran, N. (2006). Coastal mangrove forests mitigated tsunami. *Estuarine, Coastal and Shelf Science*, *65*(3), 601−606.

Kellndorfer, J., Walker, W., Perce, L., Dobson, C., Fites, J. A., Hunsaker, C., Vona, J., & Clutter, M. (2004). Vegetation height estimation from Shuttle Radar Topography Mission and National Elevation Datasets. *Remote Sensing of Environment*, *93*, 339−358.

Kovacs, J. M., Wang, J. F., & Flores-Verdugo, F. (2005). Mapping mangrove leaf area index at the species level using IKONOS and LAI-2000 sensors for the Agua Brava Lagoon, Mexican Pacific. *Estuarine Coastal and Shelf Science*, *62*, 377−384.

Laba, M., Smith, S. D., & Degloria, S. D. (1997). Landsat-based land cover mapping in the lower Yuna River watershed in the Dominican Republic. *International Journal of Remote Sensing*, *18*(14), 3011−3025.

Lefsky, M. A., Harding, D. J., Keller, M., Cohen, W. B., Carabajal, C. C., Del Bom Espirito-Santo, F., Hunter, M. O., & de Oliveira, R., Jr. (2005). Estimates of forest canopy height and aboveground biomass using ICESat. *Geophysical Reasearch Letters*, *32*.

Mancera, J. E., & Mendo, J. (1996). Population dynamics of the oyter *Crassostrea rhizophorae* from the Ciénaga Grande de Santa Marta, Colombia. *Fisheries Research*, *26*, 139−148.

Mancera, J. E., & Vidal, A. (1994). Florecimiento de microalgas relacionado con muerte masiva de peces en el complejo lagunar Ciénaga Grande de Santa Marta, Caribe colombiano. *Anales del Instituto de Investigaciones Marinas de Punta de Betín*, *23*, 103−117.

Mougin, E., Proisy, C., Marty, G., Fromard, F., Puig, H., Betoulle, J. L., & Rudant, J. P. (1999). Multifrequency and multipolarisation radar backscattering from mangrove forests. *IEEE Transactions on Geoscience and Remote Sensing*, *37*(1), 94−102.

Polania, J., Santos-Martinez, A., Mancera, J. E., & Botero, L. (2001). The coastal lagoon Cienaga Grande de Santa Marta, Colombia. In U. Seeliger & B. Kjerfve (Eds.), *(Org.). Coastal Marine Ecosystems of Latin America Ecological Studies*, *vol. 144*. (pp. 33−45). Berlin: Springer. ISBN 3540672281.

Rueda, M. (2001). Spatial distribution of fish species in a tropical estuarine lagoon: A geostatistical appraisal. *Marine Ecology Progress Series*, *222*, 217−226.

Rueda, M., & Santos-Martinez, A. (1999). Population dynamics of the striped mojarra *Eugerres plumieri* from the Cienaga Grande de Santa Marta, Colombia. *Fisheries Research*, *42*, 155−166.

Ramsey, E. W., III, & Jensen, J. R. (1996). Remote sensing of mangrove wetlands: Relating canopy spectra to site-specific data. *Photogrammetric Engineering and Remote Sensing*, *62*(8), 939−948.

Rasolofoharinoro, M., Blasco, F., Bellan, M., Azipuru, M., Gauquelin, T., & Denis, J. (1998). A remote sensing based methodology for mangrove studies in Madagascar. *International Journal of Semote Sensing*, *19*(10), 1873−1886.

Restrepo, J. D., & Kjerfve, B. (2000). Magdalena River: Interannual variability (1975–1995) and revidsed water discharge and sediment load estimates. *Journal of Hydrology*, *235*(1), 137−149.

Rivera-Monroy, V. H., Twilley, R. R., Bone, D., Childers, D. L., Coronado-Molina, C., Feller, I. C., Herrera-Silveira, J., Jaffe, R., Mancera, E., Rejmankova, E., Salisbury, J. E., & Weil, E. (2004). A conceptual framework to develop long-term ecological research and management objectives in the wider Caribbean region. *Bioscience*, *54*, 843−856.

Rivera-Monroy, V. H., Twilley, R. R., Mancera, E., Alcantara-Eguren, A., Castañeda-Moya, E., Casas, O., Reyes, P., Restrepo, J., Perdomo, L., Campos, E., Cotes, G., & Viloria, E. (2006). Aventuras y Desventuras en Macondo: Rehabilitación de la Ciénaga Grande de Santa Marta, Colombia. *Ecotropicos*, *19*, 72−93.

Rivera-Monroy, V. H., Twilley, R. R., Mancera, E., Castaneda, E., Casas, O., Daza, F., Restrepo, J., Perdomo, L., Reyes, P., Villamil, M., and Pinto, F. (2001). Estructura y función de un ecosistema de manglar a lo largo de una trayectoria de restauración en diferentes niveles de perturbación. Informe Técnico. MMA, INVEMAR, COLCIENCIAS. 331 p.

Rodriguez, E., Morris, C. S., & Beltz, J. E. (2006). A global assessment of the SRTM performance. *Photogrammetric Engineering and Remote Sensing*, *72*(3), 249−260.

Rueda, M., & Defeo, O. (2001). Survey abundance indices in a tropical estuarine lagoon and their management implications: A spatially-explicit approach. *Journal of Marine Science*, *58*, 1219−1231.

Saenger, P., & Snedaker, S. C. (1993). Pantropical trends in mangrove aboveground biomass and annual litterfall. *Oecoloia*, *69*, 263−299.

Santos-Martínez, A., & Acero, A. (1991). Fish community of the Ciénaga Grande de Santa Marta (Colombia); composition and zoogeography. *Ichthyology Explorer Freswaters*, *2*, 247−263.

Sanchez-Ramirez, C., & Rueda, M. (1999). Variacion de la diversidad de especies icticas dominantes en el Delta del rio Magdalena. *Colombia Rev. Biol. Trop.*, *vol. 47*, 1067−1079.

Schutz, B. E., Zwally, H. J., Shuman, C. A., Hancock, D., & DiMarzio, J. P. (2005). Overview of the ICEsat Mission. *Geophysical Reasearch Letters*, *32*.

Simard, M., DeGrandi, G., Saatchi, S., & Mayaux, P. (2000). Mapping tropical coastal vegetation using JERS-1 and ERS-1 radar data with a decision tree classifier. *International Journal of Remote Sensing*, *23*(7), 1461−1474.

Simard, M., Zhang, K., Rivera-Monroy, V. H., Ross, M., Ruiz, P., Castaneda-Moya, E., Rodriguez, E., & Twilley, R. (2006). Mapping mangrove height and estimate biomass in the Everglades using SRTM elevation data. *Photogrammetric Engineering and Remote Sensing*, *72*(3), 299−311.

Slater, J. A., Garvey, G., Johnston, C., Haase, J., Heady, B., Kroenung, G., & Little, J. (2006). The SRTM data fishing process and products. *Photogrammetric Engineering and Remote Sensing*, *72*(3), 237−247.

Smith, J. T., III, & Whelan, K. R. T. (2006). Development of allometric relations for three mangrove species in South Florida for use in the Greater Everglades Ecosystem restoration. *Wetlands Ecology and Management*, *14*, 409−419.

Thom, B. G. (1982). Mangrove ecology geomorphological perspective. In B. F. Clough (Ed.), *Mangrove ecosystems in Australia* Canberra: Australian National University Press.

Twilley, R. R., & Rivera-Monroy, V. H. (2005). Developing performance measures of mangrove wetlands using simulation models of hydrology, nutrient biogeochemistry and community dynamics. *Journal of Coastal Research*, *40*, 79−93.

Twilley, R. R., Rivera-Monroy, V. H., Chen, R., & Botero, L. (1998). Adapting an ecological mangrove model to simulate trajectories in restoration ecology. *Marine Pollution Bulletin*, *37*, 404−419.

UNEP-WCMC. (2006). *In the front line: Shoreline protection and other ecosystem services from mangroves and coral reefs.* Cambridge, UK: UNEP-WCMC 33 pp.

Valiela, I., Bowen, J. L., & York, J. K. (2001). Mangrove forests: One of the world's threatened major tropical environments. *Bioscience*, *51*(10), 807−815.

Wang, L., Sousa, W. P., Gong, P., & Bibging, G. S. (2004). Comparison of IKONOS and QuickBird images for mapping mangrove species on the Caribbean coast of Panama. *Remote Sensing of Environment*, *91*, 432−440.